

Fluorescence resonance energy transfer dynamics during protein folding: Evidence of multistage folding kinetics

Arnab Mukherjee and Biman Bagchi*

Solid State and Structural Chemistry Unit, Indian Institute of Science, Bangalore 560 012, India

Fluorescence resonance energy transfer (FRET) during folding of a model protein, HP-36, is investigated by Brownian dynamics simulation. Computer simulations of this protein show that folding kinetics is non-exponential and multistage, after a fast initial hydrophobic collapse. This multistage dynamics can be captured in FRET with a suitably chosen donor–acceptor pair. In particular, we find that FRET can be sensitive to late stages of changes in the radius of gyration which is found to occur for this model protein. This late stage dynamics is driven by changes in the topological pair contact formation.

FLUORESCENCE resonance energy transfer (FRET) provides a unique tool to study the dynamics of protein folding directly in the time domain. One can combine this technique with single-molecule spectroscopic techniques to obtain histograms of energy transfer efficiency which provide valuable information about the temperature and denaturant-dependent conformational states of the protein. FRET is done by attaching a donor and an acceptor at the appropriate positions along the polymer or protein molecule. On excitation of the donor molecule by a laser light, the energy transfer takes place from the donor to the acceptor. The rate of transfer and the fluorescence intensity together give information about the distance of separation between the acceptor and donor molecules. The rate of transfer is given by the well-known Förster expression¹,

$$k_f = k_{\text{rad}} \left(\frac{R_F}{R} \right)^6, \quad (1)$$

where, k_{rad} is the radiative rate and R_F is the Förster radius. By suitably choosing the donor–acceptor pair, R_F can be varied over a wide range. This allows the study of the dynamics of pair separation, essential to understand protein folding^{2,3}. k_{rad} is typically less than (but of the order of) 10^9 s^{-1} . Thus, Förster transfer provides us with a sufficiently fast camera to take snapshots of the dynamics of contact pair formation.

For flexible molecules in solution, the distance between the donor and acceptor sites is a fluctuating quantity and therefore, FRET experiments can be used to obtain detailed information on the conformational dynamics of

the individual molecules. For example, the folding dynamics of protein molecules can be studied directly using this technique. Survival probability is calculated using the FRET rate which depicts the dynamics of pair distances of the amino acid residues.

Time-resolved FRET experiments can be an important tool in understanding the folding/unfolding transitions. Lakshmikanth *et al.*⁴ performed time-resolved fluorescence with the maximum entropy method to analyse the decay kinetics, on a small protein barstar to show the existence of many equilibrium unfolding states contrary to the belief of the two-state model of protein folding. Recently, we have reported computational studies of Förster energy transfer efficiency and also dynamics of a collapsing homopolymer^{5,6}. It was found that one can use Förster efficiency distribution histograms to differentiate between different conformational states of the collapsed polymer, such as rods, toroids or simply the collapsed disordered state. In this communication, we extend the above work to study Förster energy transfer distribution and dynamics for a model protein, HP-36. We find that the results are significantly different in the case of the model protein which shows multistage dynamics that can potentially be captured by FRET.

The protein HP-36 is a thermostable subdomain of the chicken villin headpiece and it can fold autonomously to a stable structure. A large number of studies have been carried out on this protein, both using off-lattice and all-atom models^{7,8}. We have recently presented such a study using a minimalistic model^{9,10}. Construction of minimalistic potential is motivated by the hydrophobicity of different amino acid and also the different helical propensity of the amino acids residues. The structures obtained after folding resemble, to a good extent, the native state of the real protein. Interestingly, the dynamics shows a multistage folding. FRET has been calculated here along the folding trajectory between different hydrophobic residues. The dynamics of FRET reflects the multistage folding phenomenon. The histogram of the folding efficiency distribution shows interesting features.

The details of the potential is available elsewhere⁹. Here we shall present only the essential details. The model consists of two atoms for a particular amino acid. The smaller atom represents the backbone C_α atom of real protein, while the bigger atom mimics the whole side-chain residue. Basic construction of the model protein is shown in Figure 1. C_α atoms are numbered by 1, 2, 3, etc., whereas the corresponding side residues are denoted by 1', 2', 3', etc. Similar types of model (with more rigorous force field) have been introduced recently by Scheraga *et al.*^{11,12}. The total potential energy function of the model protein V_{Total} is written as,

$$V_{\text{Total}} = V_B + V_\theta + V_T + V_{LJ} + V_{\text{helix}}, \quad (2)$$

where V_B and V_θ are the potential contributions due to vibration of bonds and bending motions of the bond

*For correspondence. (e-mail: bbagchi@sscu.iisc.ernet.in)

angles. Standard harmonic potential is assumed for the above two potentials with spring constants $43.0 \text{ kJ mol}^{-1} \text{ \AA}^{-2}$ and $8.6 \text{ kJ mol}^{-1} \text{ \AA}^{-2}$ for the bonds between backbone atoms and bonds joining side residues with the backbone atoms, respectively. In case of the bending potential, spring constant is taken to be $10.0 \text{ kJ mol}^{-1} \text{ rad}^{-2}$. $V_T (= \epsilon_T \sum_{ij} \phi(1/2)[1 + \cos(3\phi)])$ is taken as the torsional potential for the rotations of the bonds. $\epsilon_T = 1 \text{ kJ mol}^{-1}$.

The nonbonding potential V_{LJ} is the sum of the pair interactions between the atoms and is given by,

$$V_{LJ} = 4 \sum_{i,j} \epsilon_{ij} \left[\left(\frac{\sigma_{ij}}{r_{ij}} \right)^{12} - \left(\frac{\sigma_{ij}}{r_{ij}} \right)^6 \right], \quad (3)$$

where r_{ij} and ϵ_{ij} are the distance and interaction between the i th and j th atom. $\sigma_{ij} = \frac{1}{2}(\sigma_{ii} + \sigma_{jj})$ and $\epsilon_{ij} = \sqrt{\epsilon_{ii}\epsilon_{jj}}$. Sizes and interactions are taken to be the same (1.8 \AA and 0.05 kJ mol^{-1} , respectively) for all the backbone atoms as they represent the C_α atoms in case of real proteins. Side residues, on the other hand, carry the characteristics of a particular amino acid. Different sizes of the side residues are taken from the values given by Levitt¹³. Interactions of the side residues are obtained from the hydrophobicities of the amino acids. So, the interaction parameters of the side residues can be mapped from the hydrophathy scale¹⁴ by using a linear equation as given below⁹,

$$\epsilon_{ii} = \epsilon_{\min} + (\epsilon_{\max} - \epsilon_{\min}) * \left(\frac{H_{ii} - H_{\min}}{H_{\max} - H_{\min}} \right), \quad (4)$$

where ϵ_{ii} is the interaction parameter of the i th amino acid with itself. $\epsilon_{\min} (= 0.2 \text{ kJ mol}^{-1})$ and $\epsilon_{\max} (= 11.0 \text{ kJ mol}^{-1})$ are the minimum and maximum values of the interaction strength chosen for the most hydrophilic (arginine) and the most hydrophobic (isoleucine) amino acid, respectively. H_{ii} is the hydrophathy index of the i th amino acid given by Kyte and Doolittle¹⁴ and H_{\min}

($= -4.5$) and $H_{\max} (= 4.5)$ are the minimum and maximum hydrophathy indices among all the amino acids. Further, details are available in ref. 9.

An important part of the secondary structure of the real protein is the formation of the α -helix. In the absence of hydrogen bonding, we introduce the following effective potential among the backbone atoms to mimic the helix formation along the chain of residues, according to the propensity of a particular amino acid and its neighbouring atoms to form a helix.

$$V_{\text{helix}} = \sum_{i=3}^{N-3} \left[\frac{1}{2} K_i^{1-3} (r_{i,i+2} - r_h)^2 + \frac{1}{2} K_i^{1-4} (r_{i,i+3} - r_h)^2 \right], \quad (5)$$

where $r_{i,i+2}$ and $r_{i,i+3}$ are the distances of the i th atom with the $i+2$ and $i+3$ th atoms, respectively. r_h is the equilibrium distance and is taken as 5.5 \AA , motivated by the observation that the distance of r_i with r_{i+2} and r_{i+3} is nearly constant at 5.5 \AA , in an α -helix. The summation excludes the first and last three amino acids, as there is less helix formation observed in the ends of the protein chain¹⁵. The force constant for the above harmonic potential is mapped from the helix propensities Hp_i taken from Pace and Scholtz¹⁶, $K_i = K_{\text{alanine}} - Hp_i \times (K_{\text{alanine}} - K_{\text{glycine}})$. K_{alanine} and K_{glycine} are the force constants for alanine and glycine, taken as 17.2 and 0.0 kJ mol^{-1} , respectively. Next, the influence of the neighbouring amino acids on the formation of the helix has been considered by taking an average of the spring constants as

$$K_i^{1-3} = \frac{1}{3} [K_i + K_{i+1} + K_{i+2}] \text{ and} \\ K_i^{1-4} = \frac{1}{4} [K_i + K_{i+1} + K_{i+2} + K_{i+3}], \quad (5)$$

with the condition that

$$K_i^{1-3}, K_i^{1-4} \geq 0,$$

as the force constant must remain positive. The above formulation of helix potential is motivated by the work of Chou and Fasman¹⁷ about the prediction of helix formation that the neighbours of a particular amino acid should be considered rather than its own helix propensity.

The initial configuration of the model protein was generated by configurational bias Monte Carlo technique¹⁸. Atoms attached to a single branch point were generated simultaneously. Then the initial configuration was subjected to Brownian dynamics simulation for the study of the folding. Time evolution of the model protein was carried out according to the motion of each bead as below,

$$\mathbf{r}_i(t + \Delta t) = \mathbf{r}_i(t) + \frac{D_i}{k_B T} \mathbf{F}_i(t) \Delta t + \Delta \mathbf{r}_i^G, \quad (6)$$

where each component of $\Delta \mathbf{r}_i^G$ is taken from a Gaussian distribution with mean zero and variance^{19,20}

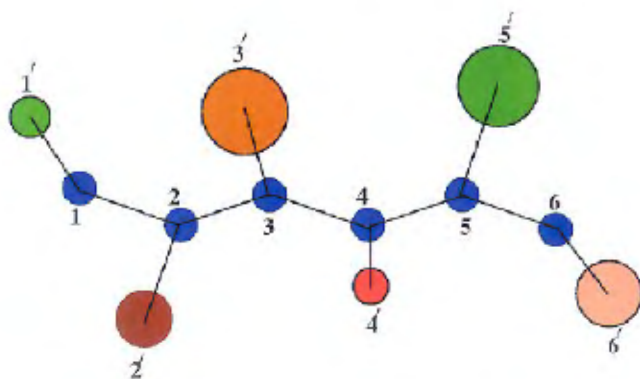


Figure 1. Construction of the model. 1 and 1' together represent an amino acid. Atoms marked with 1, 2, 3, etc. denote C_α atoms, whereas the whole side residues are denoted by atoms marked with 1', 2', 3', etc.

$$\langle(\Delta r_i^G)^2\rangle = 2D_i t,$$

$\mathbf{r}_i(t)$ is the position of the i th atom at time t and the systematic force on the i th atom at time t is $\mathbf{F}_i(t)$. The time step Δt is taken as 0.001τ . $\tau \simeq 1.2$ ns. D_i is the diffusion coefficient of the i th particle calculated from the Stokes–Einstein relation,

$$D_i = \frac{k_B T}{6\pi\eta R_i}.$$

R_i is the radius of the i th atom and η is the viscosity of the solvent. k_B and T are the Boltzmann constant and temperature, respectively. Simulations have been carried out for N number of different initial configurations, where $N = 584$.

Figure 2 presents the histogram of Förster transfer efficiency Φ_F ($= [1 + (R/R_F)^6]^{-1}$, R is the distance between donor and acceptor) both for the high-temperature unfolded and the low-temperature folded states of the model protein, with the donor and acceptor placed at 9th and 35th side-residue atoms, both of which are hydrophobic. These distributions have been obtained by calculating FRET efficiency of the equilibrium initial configurations at high temperature and the folded configurations at low temperature. The folded configurations have been generated by quenching the high temperature, extended configuration to the low temperature, collapsed configuration. FRET efficiency shows broad distributions at high temperature, as expected. However, the distribution for low-temperature folded states is rather interesting. This histogram, although shows a peak at high Förster efficiency, does show a broader tail extending up to very low efficiency. Note that the present calculation of this distribution involved a large number (584) of quenched configurations. The significant population at low efficiency shows that many of the quenched states have the donor–acceptor pair separated by significant distance. This signifies that there are many entangled and misfolded states with the residues under study lying far apart even in the low-temperature folded states, unlike in the case of homopolymers²¹. This is actually rather different from what has been reported in some experimental studies which provide a reverse description, with a relatively broad peak in the efficiency distribution for the extended states and a sharper distribution for the folded states^{22,23}.

The FRET efficiency Φ_F depends critically of the value of Förster radius R_F and the nature of donor and acceptor. Protein folding is governed mainly by the hydrophobic force. So change in FRET efficiency distribution is interesting for the hydrophobic pairs because it gives direct information about large-scale conformational change. While the broad distribution of the probability in high temperature is expected due to a flat energy surface, the distribution at low temperature signifies the misfolded and trapped states signifying a rather complicated potential energy landscape for this model protein.

Figure 3 shows the time dependence of survival probability $S_p(t)$ in FRET using Förster energy transfer rate eq. (1) for the 9–35 pair along the Brownian dynamics trajectory leading to the most stable structure. The Förster radius R_F is taken as 10 \AA . The dynamics of FRET shows initial, very slow decrease of $S_p(t)$ to be followed by a sudden drop at around 2400τ , as seen in case of the different dynamical properties discussed below. $S_p(t)$ is found to be relatively insensitive to k_{rad} .

The time dependence shown in Figure 3 can be understood from Figure 4, where the variation of the radius of gyration is plotted against time. The multistage folding process can be easily understood by monitoring the radius

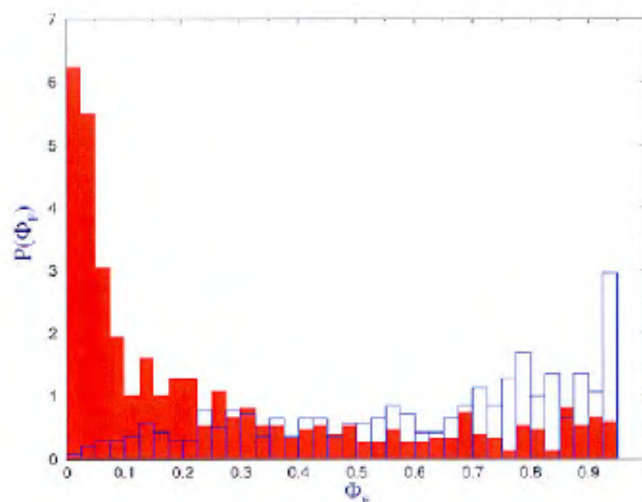


Figure 2. Probability distribution of FRET efficiency of 9–35 side-residue pairs is plotted for both high (filled histogram) and low temperature (unfilled histogram) configurations for $R_F = 20 \text{ \AA}$.

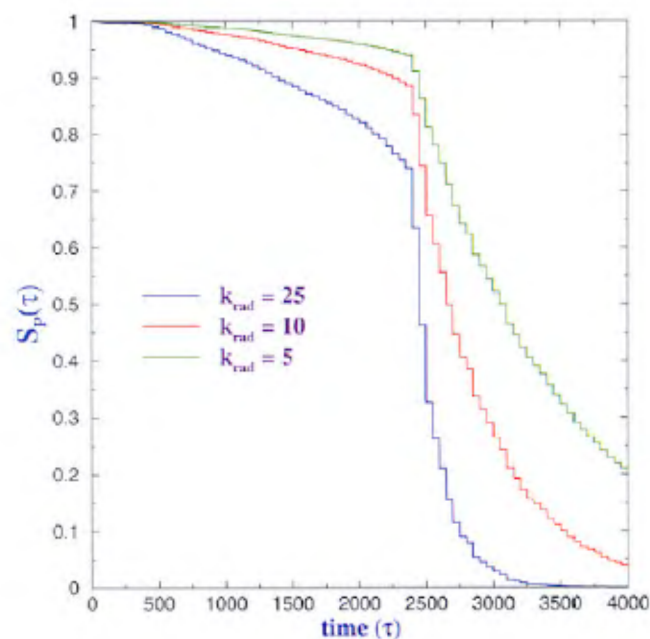


Figure 3. FRET survival probability of 9–35 side-residue pair for different radiative rates at $R_F = 10.0 \text{ \AA}$.

of gyration of the model protein with time. Consistent with the dynamics of FRET, there is a long plateau observed at the final stage of folding. This could be correlated with the underlying landscape of the model protein. The long plateau could have arisen because of the entropic bottleneck created by the large number of conformations at that particular energy level and thus delay the folding process by an enormous amount. It is interesting to note that FRET is sensitive to the slow dynamics that occurs after reduced time 2000τ and thus to the dynamics of topological pair contact formation. This is due to our choice of $R_F = 10 \text{ \AA}$, which is also the plateau value of the radius of gyration in Figure 4.

Figure 5 shows the different stages of decrease in the potential energy of the model protein (E_N) with time. There is an initial collapse followed by a slower decay which continues till 500τ . Subsequently, a long tail appears which carries out the final stage of folding and

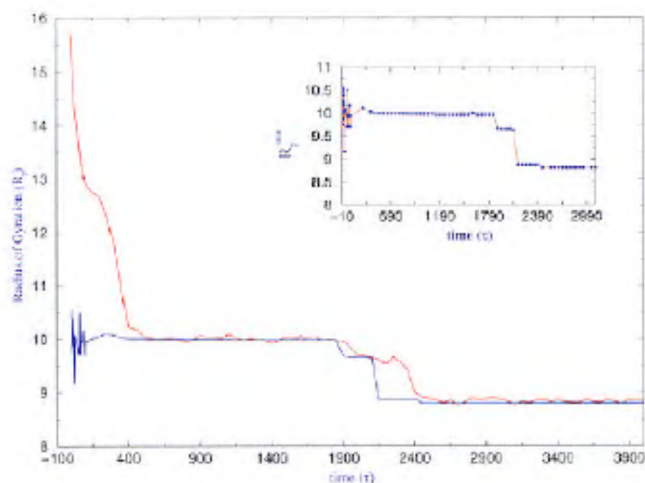


Figure 4. Solid line shows the decrease in radius of gyration (R_g) of model HP-36 with time τ . $\tau = 0$ corresponds to the time of temperature quench. (Inset) Circles with dashed line show the R_g^{min} for the corresponding minimized configurations.

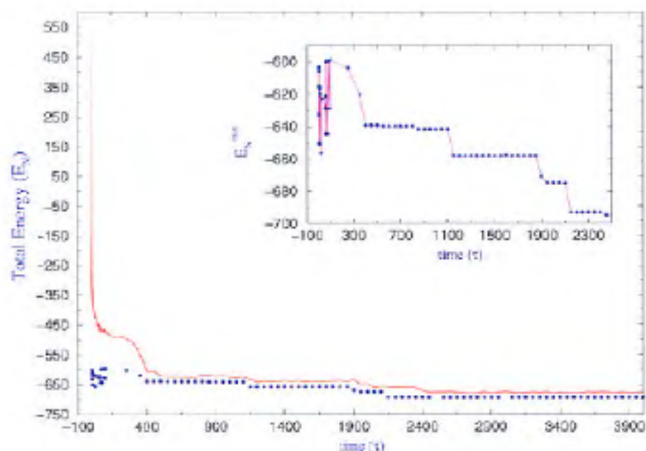


Figure 5. Solid line shows the variation of energy of model HP-36 with time subsequent to the temperature quench. Circles show the minimized energies corresponding to a particular energy value at a certain time. (Inset) Magnified plot of the change in minimized energy during folding.

the decay completely at around 2400τ . Note that FRET is not sensitive to the dynamics of energy variation.

The comparison between the folded structure of the model protein and native structure of the real protein is shown in Figure 6. Among many different folded structures, the above shows the structure with the lowest RMSD (root mean square deviation) of 4.5 \AA , calculated among the backbone of the model and real structures. The model structures show that even in the minimalistic description of a protein, the structural aspect of folding can also be understood to a certain extent.

In this communication we have presented a computational study of the Förster energy transfer dynamics during the folding of a model protein. The folding has been

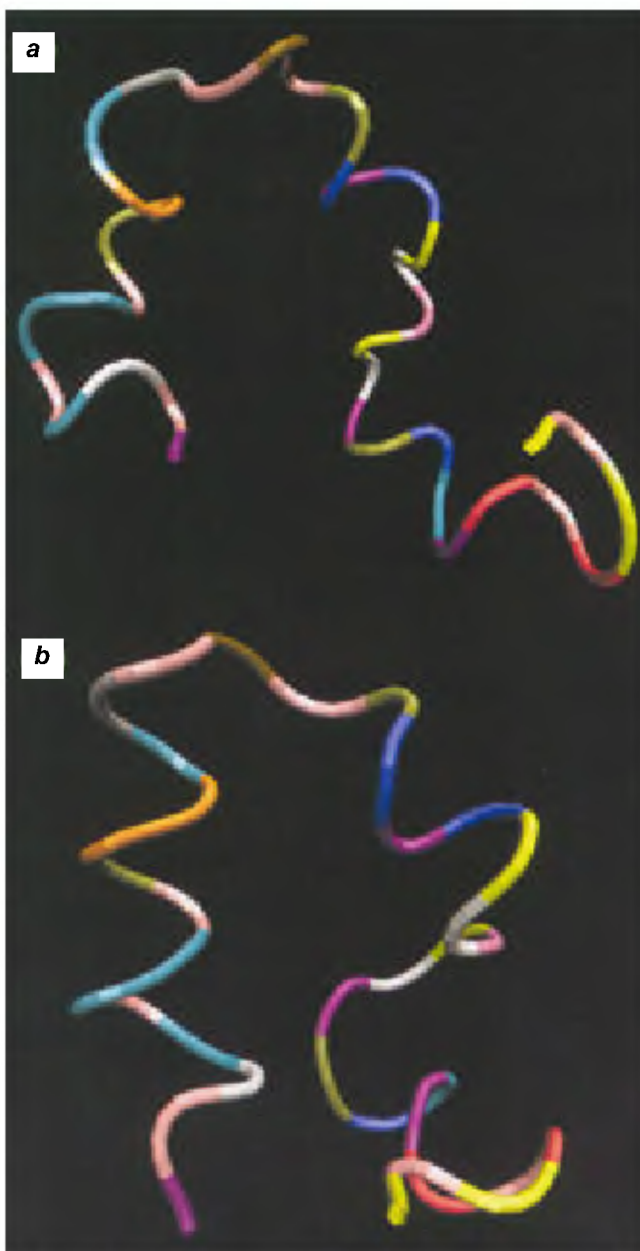


Figure 6. *a*, Backbone structure of the model protein with the lowest RMSD (4.5 \AA); *b* Backbone structure of the native state of real HP-36.

initiated by quenching the protein from a high temperature to a low temperature. The dynamics of folding is found to occur in stages, reflecting the rugged energy landscape that the folding faces. This ruggedness is to be contrasted with the nearly smooth landscape that we found for models with simpler potentials. The FRET efficiency at low temperature shows a broad distribution signifying many trapped and misfolded states which may originate from the underlying rugged energy landscape. The multistage dynamics is reflected in the decay of survival probability. In particular, FRET is sensitive to the late stage of changes in the radius of gyration. This late stage dynamics is driven mainly by the change in topological pair-contact formation.

1. Förster, Th., Zwischenmolekulare energiewanderung und fluoreszenz. *Ann. Phys. (Leipzig)*, 1948, **2**, 55–75.
2. Telford, J. R., Wittung-Stafshede, P., Gray, H. B. and Winkler, J. R., Protein folding triggered by electron transfer. *Acc. Chem. Res.*, 1998, **31**, 755–763; Pascher, T., Chesick, J. P., Winkler, J. R. and Gray, H. B., Protein folding triggered by electron transfer. *Science*, 1996, **271**, 1558–1560.
3. Lyubovitsky, J. G., Gray, H. B. and Winkler, J. R., Mapping the cytochrome C folding landscape. *J. Am. Chem. Soc.*, 2002, **124**, 5481–5485.
4. Lakshmikanth, G. S., Sridevi, K., Krishnamoorthy, G. and Udgaonkar, J. B., Structure is lost incrementally during the unfolding of barstar. *Nat. Str. Biol.*, 2001, **8**, 799–804.
5. Srinivas, G. and Bagchi, B., Detection of collapsed and ordered polymer structures by fluorescence resonance energy transfer in stiff homopolymers: Bimodality in the reaction efficiency distribution. *J. Chem. Phys.*, 2002, **116**, 837–844.
6. Srinivas, G., Yethiraj, A. and Bagchi, B., FRET by FET and dynamics of polymer folding. *J. Phys. Chem.*, 2001, **B105**, 2475–2478.
7. Duan, Y. and Kollman, P. A., Pathways to a protein folding intermediate observed in a 1-microsecond simulation in aqueous solution. *Science*, 1998, **282**, 740–744.
8. Fernandez, A., Shen, M., Colubri, A., Sosnick, T. R., Berry, R. S. and Freed, K. F., Large-scale context in protein folding: villin headpiece. *Biochemistry*, 2003, **42**, 664–671.
9. Mukherjee, A. and Bagchi, B., Correlation between rate of folding, energy landscape, and topology in the folding of a model protein HP-36. *J. Chem. Phys.*, 2003, **118**, 4733.
10. Mukherjee, A. and Bagchi, B., Multistage contact pair dynamics during folding of model proteins. *J. Chem. Phys.* (submitted).
11. Liwo, A., Oldziej, S., Pincus, M. R., Wawak, R. J., Rackovsky, S. and Scheraga, H. A., A united-residue force field for off-lattice protein-structure simulations. I. Functional forms and parameters of long-range side-chain interaction potentials from protein crystal data. *J. Comput. Chem.*, 1997, **18**, 8849–8873.
12. Scheraga, H. A. *et al.*, Recent improvements in prediction of protein structure by global optimization of a potential energy function. *Proc. Natl. Acad. Sci. USA*, 2001, **98**, 2329–2333; Lee, J., Liwo, A. and Scheraga, H. A., Conformational space annealing and an off-lattice united-residue force field: application to the 10–55 fragment of staphylococcal protein A and to apo calbindin D9K. *Proc. Natl. Acad. Sci. USA*, 1999, **96**, 2025–2030.
13. Levitt, M. and Warshel, A., Computer simulation of protein folding. *Nature*, 1975, **253**, 694–698; Levitt, M., A simplified representation of protein conformations for rapid simulation of protein folding. *J. Mol. Biol.*, 1976, **104**, 59–107.
14. Kyte, J. and Doolittle, R. F., A simple method for displaying the hydrophobic character of a protein. *J. Mol. Biol.*, 1982, **157**, 105–132.
15. Zimm, B. H. and Bragg, J. K., Theory of the phase transition between helix and random coil in polypeptide chains. *J. Chem. Phys.*, 1959, **31**, 526–535.
16. Pace, C. N. and Scholtz, J. M., A helix propensity scale based on experimental studies of peptides and proteins. *Biophys. J.*, 1998, **75**, 422.
17. Chou, P. Y. and Fasman, G., Conformational parameters for amino acids in helical, beta-sheet, and random coil regions calculated from proteins. *Biochemistry*, 1974, **13**, 211–222.
18. Mooij, G. C. A. M., Frenkel, D. and Smit, B., Direct simulation of phase equilibria of chain molecules. *J. Phys. Condens. Matter*, 1992, **4**, L255–L259; Frenkel, D. and Smit, B., Unexpected length dependence of the solubility of chain molecules. *Mol. Phys.*, 1992, **75**, 983–988.
19. Ermak, D. L. and McCammon, J. A., Brownian dynamics with hydrodynamic interactions. *J. Chem. Phys.*, 1978, **69**, 1352–1360.
20. Hansen, J. P. and McDonald, I. R., *Theory of Simple Liquids*, Academic Press, 1986.
21. Deniz, A. A. *et al.*, Single molecule protein folding: diffusion Forster energy transfer studies of the denaturation of Chymotrypsin inhibitor 2. *Proc. Natl. Acad. Sci. USA*, 2000, **97**, 5179–5184.
22. Deniz, A. A. *et al.*, Radiometric single pair FRET on freely diffusing molecules – observation of Forster distance dependence and of sub-populations. *Proc. Natl. Acad. Sci. USA*, 1999, **96**, 3670–3675.
23. Srinivas, G. and Bagchi, B., Energy transfer efficiency distributions in polymers in solution during folding and unfolding. *Phys. Chem. Commun.*, 2002, **5**, 59–62.

ACKNOWLEDGEMENTS. We thank CSIR, DAE and DST, New Delhi for financial support. A.M. thanks Ashwin, Kausik, Prasanth, Rajesh, Dwaipayan and Swapan for help and discussions.

Received 28 March 2003; revised accepted 21 May 2003

Electrodynamic confinement of europium ions

Pushpa M. Rao*, Soumen Bhattacharya, S. G. Nakhate and Gopal Joshi[†]

Spectroscopy Division, [†]Electronics Division, Bhabha Atomic Research Centre, Mumbai 400 085, India

Europium ions were trapped in a Paul trap. The trapped ions were detected electronically, which involved the damping of a weakly excited tank circuit across the trap electrodes, tuned to one of the ion frequencies in the trap. The storage time of the trapped ions was observed to be 8 s at 2.4×10^{-6} Pa base vacuum. On cooling the ions with nitrogen as buffer gas at 1.8×10^{-4} Pa and helium at 6.4×10^{-5} Pa, the storage time improved to 41.4 s and 102.7 s respectively.

THE confinement of an ensemble of free ions allowing the observation of isolated charge particles, even that of a single ion requires novel techniques as reported in *The technique of ion trapping*. During the last two decades, there has been a tremendous progress in the techniques of trapping and cooling of ions in the quadrupole ion traps. A single ion has been trapped and observed over a long period of time enabling the measurement of its properties with an extremely high accuracy in the fields of atomic physics, quantum optics and nuclear physics^{1–4}.

*For correspondence. (e-mail: pushpam@magnum.barc.ernet.in)